Continental Shelf Research 111 (2015) 112–125

Contents lists available at ScienceDirect

Continental Shelf Research

journal homepage: www.elsevier.com/locate/csr

Research papers

River-derived sediment suspension and transport in the Bohai, Yellow, and East China Seas: A preliminary modeling study

Xiangming Zeng [a], Ruoying He [a,*], Zuo Xue [b,c,d], Houjie Wang [e], Yue Wang [f], Zhigang Yao [f], Weibing Guan [g], Jennifer Warrillow [a]

[a] Department of Marine, Earth, and Atmospheric Sciences, North Carolina State University, Raleigh, NC, USA
[b] Department of Oceanography and Coastal Sciences, Louisiana State University, Baton Rouge, LA, USA
[c] Center for Computation and Technology, Louisiana State University, Baton Rouge, LA, USA
[d] Coastal Studies Institute, Louisiana State University, Baton Rouge, LA, USA
[e] College of Marine Geosciences, Ocean University of China, Qingdao, China
[f] Physical Oceanography Laboratory, Ocean University of China, Qingdao, China
[g] State Key Laboratory of Satellite Ocean Environment Dynamics, Second Institute of Oceanography, State Oceanic Administration, Hangzhou, China

ARTICLE INFO

Article history:
Received 23 March 2015
Received in revised form
22 July 2015
Accepted 17 August 2015
Available online 22 August 2015

Keywords:
Huanghe River
Changjiang River
Sediment transport
Wave–current coupling

ABSTRACT

Coastal circulation and transport of sediment derived from the Huanghe and Changjiang Rivers in the Bohai, Yellow, and East China Seas (BYECS) over the past 48 years (1958–2005) were simulated and analyzed using the Coupled Ocean–Atmosphere–Wave–Sediment Transport modeling system. Model skill assessments against in situ wave and hydrographical observations indicate the model simulation can reasonably well reproduce the hydrodynamic environment of the BYECS. Model-simulated regions of high fine sediment accumulation rate correlate well with the observed regions, which are known as "muddy patches." Bottom stress analysis further indicates that the formation of muddy patches near river mouths is largely due to their proximity to the sediment source. Muddy patches formed in regions farther away from river mouths are results of local weak bottom stress and associated circulation pattern. Simulated seabed sediment distribution reveals that most of the Huanghe-derived sediment stays inside the Bohai Sea, whereas the Changjiang-derived sediment can spread into both the Yellow and East China Seas. Strong seasonal variations exist in the river-derived sediment transport with stronger (weaker) offshore sediment transport occurring in the winter (summer).

1. Introduction

The Bohai, Yellow, and East China Seas (BYECS), consisting of a semi-closed basin in the north and a wide continental shelf in the south, are one of the largest continental systems in the world (Lin et al., 2002; Fig. 1a). The Bohai Sea (BS) is connected to the Yellow Sea (YS) through the Bohai Strait between the Liaodong and Shandong Peninsulas. The mean depth of the BS is only ~18 m. Mean tidal currents vary from 0.2 to 0.8 m/s and are dominated by mixed semi-diurnal tides (M_2 and S_2; Huang et al., 1999). Because of the shallow depth, wind waves can affect almost the entire basin, with a typical significant wave height varying from 0.3 to 0.7 m near the coast to about 1.0 m in the Bohai Strait and central basin (Jiang et al., 2000). The mean circulation in the BS consists of an inflow through the northern section of the Bohai Strait and an outflow through the southern part (Guan, 1994).

In the Yellow Sea (YS), the mean water depth is ~44 m. The regional tidal system is dominated by M_2 and K_1 (Naimie et al., 2001) and rotates in a counterclockwise direction. Typical tidal current speed is less than 0.45 m/s in the middle YS, but increases to more than 1.5 m/s near the coast. In the northern YS, waves are generally wind-generated, while the southern YS is more affected by waves propagating from the open ocean. Overall, the typical significant wave height is largest in fall and winter (2.0–6.0 m), and smallest in spring and summer (0.4–1.2 m). Circulation in the YS has obvious seasonal variation. In winter, the strong Yellow Sea Warm Current (YSWC) flows northward through the middle of the YS, while the relatively weak Yellow Sea Coastal Current (YSCC) and the Korean Coastal Current (KCC) flow southward. In contrast, the YSWC becomes very weak in summer, only reaching north of Cheju Island before turning eastward into the Cheju Strait between Cheju Island and the Korean Peninsula (Lie, 1986; Park, 1986; Su, 2001). Both the YSCC and KCC flow north during that time (Xia et al., 2006; Bian et al., 2013a).

The East China Sea (ECS) connects to the YS in the north and to the western Pacific Ocean in the southeast by the Okinawa Trough.

* Corresponding author.
E-mail address: rhe@ncsu.edu (R. He).

http://dx.doi.org/10.1016/j.csr.2015.08.015
0278-4343/

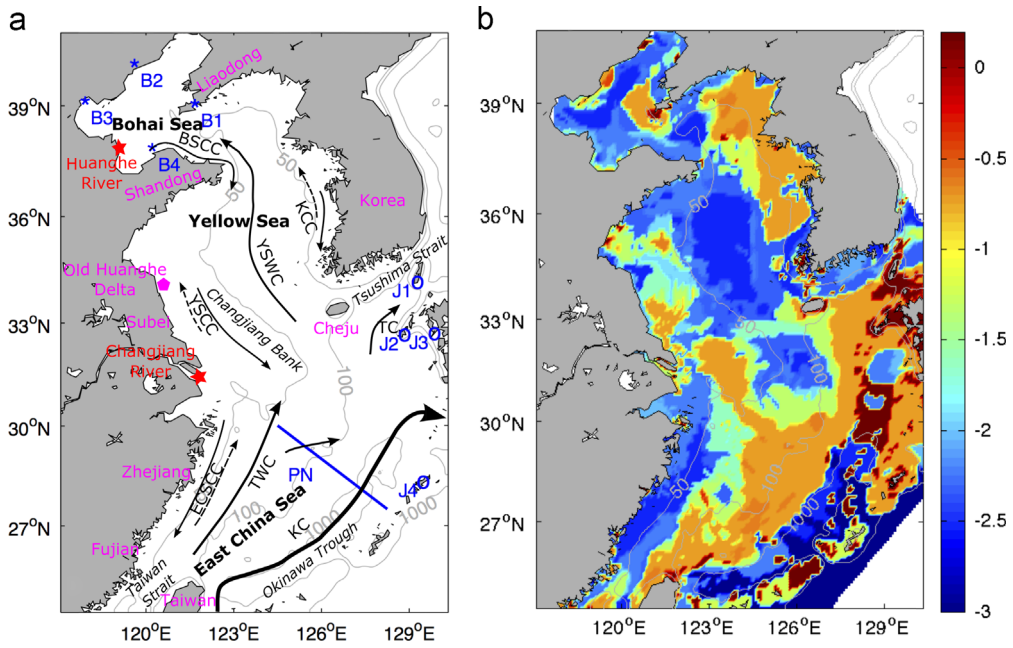

Fig. 1. Schematic illustration of (a) currents and (b) median grain size distribution (scale: log 10 mm) of seabed sediment. Gray contours are 50, 100, and 1000 m isobaths. (a) Solid arrows indicate the Bohai Sea Coastal Current (BSCC), Korean Coastal Current (KCC), Yellow Sea Warm Current (YSWC), Yellow Sea Coastal Current (YSCC), East China Sea Coastal Current (ECSCC), Taiwan Warm Current (TWC), Tsushima Current (TC), and Kuroshio Current (KC). The dashed arrows represent the KCC, YSCC, and ECSCC in summer. Five-pointed stars mark the river mouths of the Huanghe and Changjiang Rivers. The pentagon is the position of the Old Huanghe River Delta. The four blue stars (B1, B2, B3, and B4) in the Bohai Sea are stations for temperature comparison, while the four blue circles (J1, J2, J3, and J4) are the sea level validation stations. The blue line is the PN transect for temperature and salinity comparison. (b) Grain size data come from the digitized seabed sediment distribution map (Li et al., 2005a).

It has a broad continental shelf with mean depth of 72 m (Dong et al., 2011). The M_2 tidal constituent dominates the ECS tidal system. The tidal amplitude can reach 5 m at the Zhejiang–Fujian coast, and the speed of tidal currents is 0.4–1.0 m/s. Waves in the southern ECS are generally larger than those in the north. The nearshore East China Sea Coastal Current (ECSCC), driven by seasonal winds, flows southward in winter and northeastward in summer. Circulation on the ECS continental shelf is very dynamic, and is influenced by the interplay among the South China Sea through the Taiwan Strait, the YS through YSCC, the large freshwater input from the Changjiang River, and the strong western boundary current-Kuroshio Current (KC), with a surface current speed around 1 m/s (Pan et al., 1987a,1987b).

River-derived sediment is a major source of material transported to the BYECS (Milliman and Meade, 1983). As the two largest rivers in east Asia, the Huanghe (Yellow) and Changjiang (Yangtze) Rivers deliver annually about 1.1×10^9 and 4.8×10^8 t sediment, respectively, into the BYECS (Milliman and Meade, 1983; Saito and Yang, 1995; Fig. 1a). Waste and contaminants from human activities are included in the sediment, and carried to adjacent oceans by the two rivers (e.g. Qiao et al., 2007). Because of this huge sediment supply and its potential impact on the coastal environment and marine ecosystem, sediment transport in the BYECS has been a subject of many earlier studies (Choi, 1983; Dong et al., 1989; Milliman et al., 1985a, 1985b; Deng and Yang, 1993; Zhang, 1995; Wu et al., 2001; Ma et al., 2001; Lin et al., 2002; Wang et al., 2007a; Li, 2008; Dong et al., 2011; Zeng et al., 2011; Milliman and Yang, 2014).

Existing observations of sediment distribution on the seabed show that over broad areas of the BYECS continental shelf, "old" sand deposited during the last glacial maximum when sea level was low (Emery, 1968). Isolated areas of fine-grain modern sediment, known as "muddy patches", are present in the western BS, northeast of the Shandong Peninsula, in the YS Trough, at the Old Huanghe River Delta, southeast of the Changjiang Estuary, southwest of Cheju Island, in the Okinawa Trough, and along the Zhejiang–Fujian coast (Qin, 1994; Saito and Yang, 1995; Liu et al., 2002, 2006, 2007, 2009; Fig. 1b). This fine-grain sediment is believed to be transported from rivers in the area, as the modern coarse-grain accumulation rate in these areas is small (DeMaster et al., 1985).

The seabed in the BS is dominated by sediment derived from the Huanghe River (Wang et al., 2014), while the Changjiang River-derived sediment is considered to be the major source of muddy patches near the Changjiang Estuary and the Zhejiang–Fujian coast (Hu et al., 2001; Xiao et al., 2005; Xu et al., 2009). The large sediment input from these rivers contributes significant amounts of nutrients and contaminants from land adjacent to the seas, and these play an important role in controlling the physical and biogeochemical environment of the BYECS (Hu et al., 2011; Dong et al., 2011; Xu et al., 2012). However, due to the complex physical environment and a lack of observations, understanding regional seabed sediment distributions, transport pathways, and their seasonal variations remains a very challenging task.

In recent years, numerical models have been used as a powerful tool for sediment transport studies around the world. Jiang et al. (2004) used both field experiments and numerical simulations to study suspended particulate matter transport in the BS. Wang et al. (2007b) and Harris et al. (2008) studied sediment transport and resuspension in the northern Adriatic Sea, respectively. Also in Adriatic Sea, Bever et al. (2009) investigated the fate of Po River sediment within the basin, and Sclavo et al. (2013) focused on the effect of wave–current interaction on sediment dispersal. Warner et al. (2008a) simulated sediment transport during storms in Massachusetts Bay. Lu et al. (2011) applied a current–wave coupled model to study transport dynamics and seasonal variability of Huanghe River sediment in the BS and YS. Xu et al. (2011) investigated the dispersal of Mississippi and Atchafalaya River sediment on the Texas–Louisiana shelf. Xue et al. (2012) applied a coupled wave–ocean–sediment transport model to reveal the

sediment transport mechanisms of the Mekong River. Most recently, Bian et al. (2013a) explored the sediment transport path and dynamics in the BYECS under climatological mean circulation and wind forcing. Regional circulation is known to be strongly influenced by the synoptic weather patterns, especially in the winter season (Yuan et al., 2008). Sediment transport forced by synoptic forcing over a longer period, along with accounting for of interactions of ocean currents with the wave dynamics present areas of future improvement. In addition, Bian et al. (2013b) presented the distribution of suspended sediment concentration in the YS and ECS based on field surveys during the four seasons of 2011.

While most sediment transport modeling studies carried out in the BYECS focused on smaller sub-regions with relatively simple physical settings over short time periods (from days to a few years), it is our goal to investigate intrinsic seasonal and interannual variability in Huanghe and Changjiang River-derived sediment transport mechanisms in the entire BYECS over a longer time period. To do that, we have applied an advanced coupled ocean-wave-sediment transport model-COAWST (Coupled–Ocean–Atmosphere–Wave–Sediment Transport Modeling System) to simulate realistic hydrodynamic settings and transport of riverine sediment in the BYECS over 48 years (1958–2005). We provide herein our model setup, validations, and analyses of seasonal variations in sediment transport in this work. Results and analyses of the interannual variability will be reported in a future correspondence.

2. Model

Our coupled modeling system (Warner et al., 2008b, 2010) consists of several state-of-the-art modeling components, including the Regional Ocean Modeling System (ROMS, Shchepetkin and McWilliams, 2005; Haidvogel et al., 2008; Schepetkin and McWilliams, 2009) for ocean and sediment transport, and the Simulating Waves Nearshore (SWAN) model (Booij et al., 1999) for ocean waves. Model coupling is handled through the Model Coupling Toolkit (MCT, Larson et al., 2005). As ROMS and SWAN run simultaneously, ROMS passes bottom elevation, sea surface height, and depth-averaged currents to SWAN, and SWAN passes wave direction, height, length, period, and energy dissipation to ROMS. Because our focus is on long-term sediment transport, by coupling waves with ocean circulation, the model system accounts for wave-induced enhancement of surface roughness, water column mixing, and bottom stress, all of which are critical to sediment transport. For example, the total bottom stress τ_t used for sediment transport algorithm in the model is related to bed stresses associated with mean current above the wave-boundary layer τ_c and wave motion τ_w implemented through a bottom-boundary layer model (Madsen, 1994; Warner et al., 2008b). The estimates of τ_c and τ_w are made as $\tau_c = (u^2 + v^2)k^2/\ln^2(z/z_0)$ and $\tau_w = 0.5 f_w u_b^2$, respectively, where u and v are velocity computed at the vertical mid-elevation of the bottom computational cell, k is von Kármán's constant, z is the vertical mid-elevation point of the bottom cell, z_0 is the bottom roughness length, f_w is the Madsen wave-friction factor, and u_b is the bottom orbital velocity (Warner et al., 2008b). More details about the bottom-boundary layer model, model coupling, and wave–current interaction can be found in Warner et al. (2008b, 2010), Olabarrieta et al. (2011), Kumar et al. (2012), and Sclavo et al. (2013).

In this study, the model domain covers the whole BYECS, with 1/12° grid spacing horizontally and 16 terrain-following layers vertically to resolve the water column. ETOPO2 global topography data with 2-min spatial resolution (National Geophysical Data Center, 2006), from the National Oceanic and Atmospheric Administration (NOAA), was used to define model bathymetry. Without compromising our goal of studying sediment transport on the BYECS shelf, we set the least and largest water depths as 5 m and 1200 m, to increase the stability and efficiency of model integration. Warner et al. (2005) reviewed and compared different turbulence closure schemes in ocean circulation modeling. The Mellor–Yamada 2.5 Turbulence Closure scheme was used in this study to represent vertical mixing (Mellor and Yamada, 1982), because we found numerically it is the most stable scheme for our multi-decadal long simulation. At the surface, the model was forced by daily wind and net surface heat flux interpolated from National Centers for Environmental Prediction (NCEP) Reanalysis data products with 1-degree spatial resolution (Kalnay et al., 1996). At the two open boundaries (south and east) of our model, quarter-degree monthly Simple Ocean Data Assimilation (SODA, Carton et al., 2000a, 2000b) solutions were used to define sea level, transport, and temperature and salinity boundary conditions. To introduce tidal dynamics, eight major tidal constituents (M_2, S_2, N_2, K_2, K_1, O_1, P_1 and Q_1) derived from the OSU TOPEX/Poseidon Global Inverse Solution (Egbert et al., 1994; Egbert and Erofeeva, 2002) were superimposed on the SODA subtidal sea level and transport values along the open boundaries. To improve the stability of the long-term circulation model integration, we introduced the Orlanski-type radiation (Orlanski, 1976) for three-dimensional temperature, salinity and current fields along the southern boundary, so any spurious waves generated in the model interior can freely propagate outside our study domain. Moreover, temperature and salinity values along the eastern boundary were clamped to SODA counterparts in order to maintain the intensity and structure of the KC. The wave model used the same 1/12°

Table 1
Sediment parameter settings.

	Fine	Coarse
Diameter (mm)	0.0039	0.015
Settling velocity (mm/s)	0.1	0.4
Critical shear stress (N/m^2)	0.02	0.07
Density (kg/m^3)	2650	2650
Surface erosion rate (kg/m^2/s)	0.00002	0.00002
Porosity	0.4	0.4

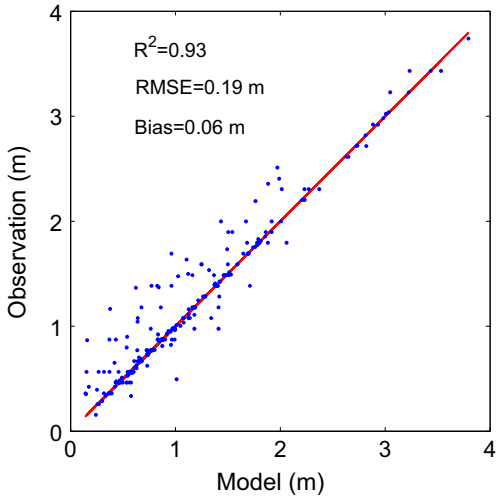

Fig. 2. Comparisons between observed and modeled monthly mean significant wave height during 1993–2005. Observations are from Globalwave TOPEX altimeter along-track (L2P) data. Solid line is the line of perfect match. R^2 represents the coefficient of determination. RMSE is root mean square error.

horizontal grid, bathymetry, and meteorological forcing as the ocean model. We focused on the wind waves generated inside the study domain, and no open-ocean wave boundary forcing was considered. Coupled model variables, including significant wave height, wave length, wave direction, bottom orbital velocity and surface currents were exchanged between SWAN and ROMS daily.

In the sediment module, we considered only two classes of river-derived sediment: fine and coarse, for simplicity. The corresponding parameters used in the model are listed in Table 1, following Bian et al. (2013a). Only the Huanghe and Changjiang Rivers were included as sediment sources (with different flags) in our study. Their runoff accounts for ~4% and 80% of total riverine input in the BYECS, respectively, whereas the sediment discharge accounts for ~65% and 30%, respectively (Ichikawa and Beardsley, 2002; Yang et al., 2003; Xu et al., 2009; Liu et al., 2013). The river runoff and sediment discharge values were interpolated from observed monthly records of two long-term gauge stations-Lijin (~100 km upstream of Huanghe River mouth) and Datong (~500 km upstream of Changjiang River mouth). To account for sediment deposition difference between gauge stations and river mouths, we set the sediment input from the two rivers to be 70% of their upstream gauge observations, while keeping the runoff rate unchanged, following Li et al. (2005b). Although other researchers tried to estimate the component of different sediment classes (e.g. Bonaldo and Di Silvio, 2013), it is difficult to do so for the Huanghe and Changjiang Rivers due to different geographic and hydrodynamic environment. As a result, the fraction of fine and coarse sediment was simply set at 50% each, following Bian et al. (2013a). Seabed evolution was also considered in this model. Deposition is modeled and represented by sediment concentration on the seabed, which is a three-dimensional array with user-defined constant layers beneath each horizontal hydrodynamic model cell. The seabed layer thickness was modified at each time step, accounting for erosion and deposition. Initially, the

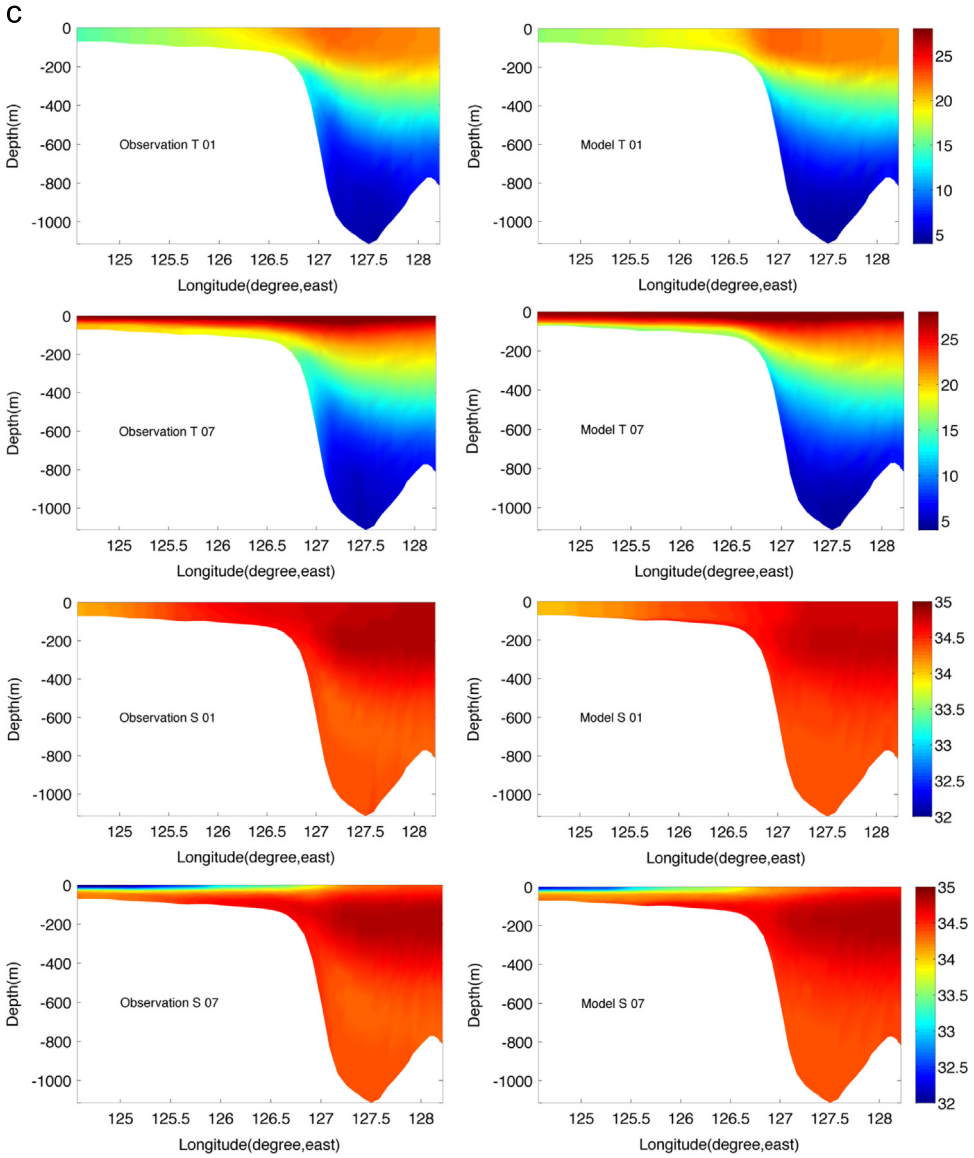

Fig. 3. Model validation. (a) Sea level anomaly comparisons between model and observations at stations J1–J4 (see Fig. 1a for locations). Correlation coefficients (r) and root mean square errors (RMSE) are given in the titles. (b) Sea surface temperature comparisons at B1–B4 (see Fig. 1a for locations). Correlation coefficients (r) and RMSEs are given in the titles. (c) Monthly averaged (January="01" and July="07") temperature (T, °C) and salinity (S) comparisons at depth along the PN transect (see Fig. 1a for location).

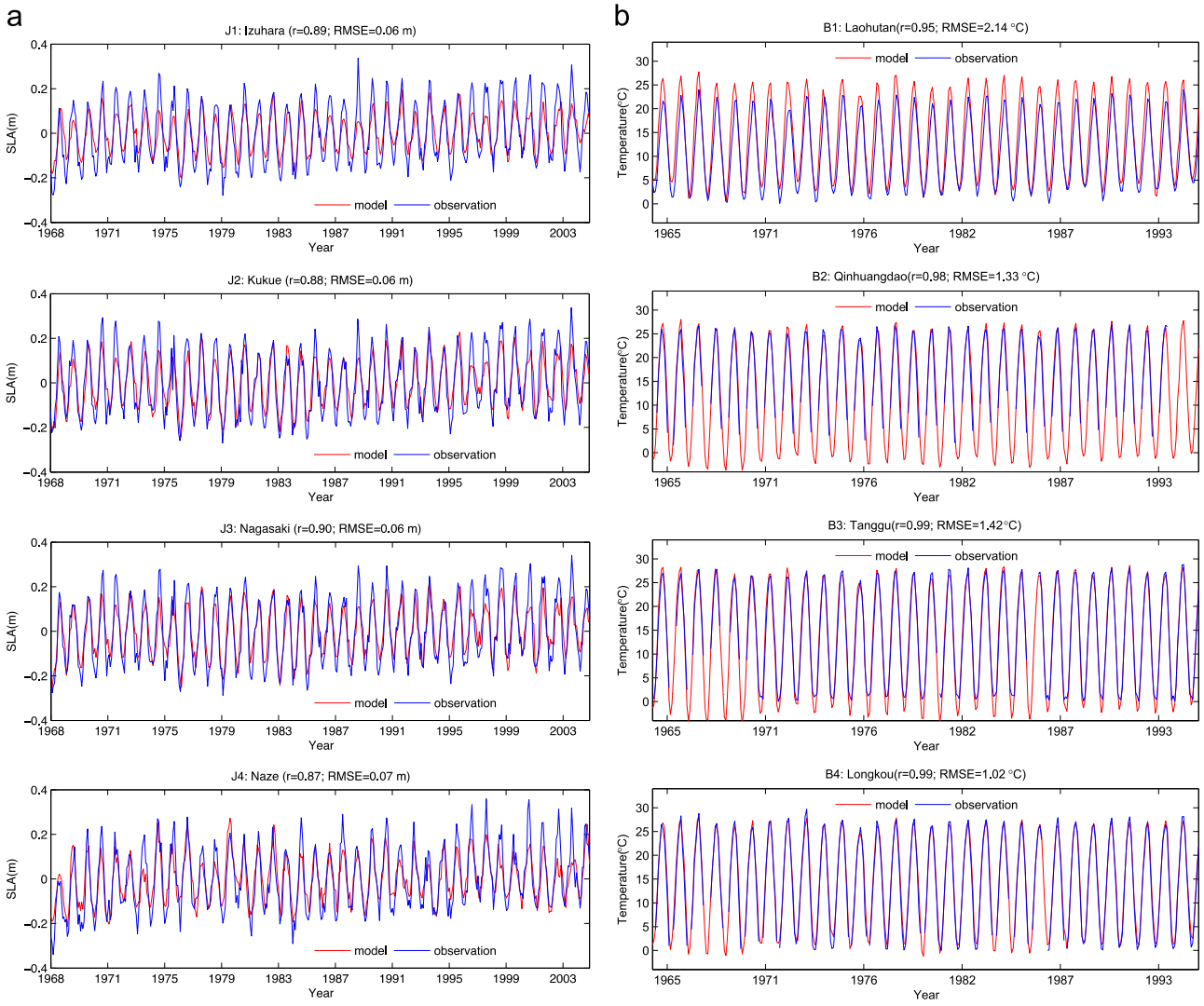

Fig. 3. (*continued*)

suspended sediment concentration in the water column was zero, and there was no sediment on the seabed; therefore in the model simulation, any deposition (or the formation of muddy patches) on the shelf was a direct result of transport of riverine sediment from the coast. The time step used for the baroclinic mode of model simulation was 300 s. The model was integrated for 48 years from Jan. 1, 1958 to Dec. 31, 2005.

3. Results and discussion

3.1. Model validation

In order to validate the wave model results, we compared the available Globalwave TOPEX/POSEIDON altimeter along-track (L2P) data (http://globwave.ifremer.fr/products/globwave-satellite-data/altimeter-l2p-data), which overlapped with the model-simulated monthly significant wave height output from 1993 to 2005. Because of the large uncertainty of TOPEX/POSEIDON observations near the coast and because we did not consider wave propagation from outside the study domain, data near the model open boundaries and coastlines were excluded from the validation. The resulting comparison shows that the simulated significant wave height agreed well ($R^2=0.93$) with the altimeter observations (Fig. 2), indicating that the model is capable of reasonably well reproducing wave conditions during the comparison period.

Coastal sea level data archives from the Japan Oceanographic Data Center (http://www.jodc.go.jp/data/tide/sea-level.html) made it possible to assess the model's skill in reproducing long-term (from 1968 to 2005) sea level variability (Fig. 3a). At all four stations (J1–J4 in Fig. 1a), the correlation coefficients between observed and modeled sea level time series are all larger than 0.87. Although relevant misfit occasionally occurs in peaks and troughs, the root mean square errors (RMSE) are small ($\lesssim 0.07$ m). The misfit is likely due to unrepresented dynamical process in coastal region by current model resolution (1/12°) and the coarse resolution of atmospheric forcing (1°). We also compared the simulated sea surface temperatures (SST) with long-term observations (Wang, 2009) from four stations (B1–B4 in Fig. 1a) in the BS (Fig. 3b). Correlation coefficients between observed and simulated SST for the four stations are above 0.95 with RMSE less than 2.14 °C, indicating that the SST variation simulated by the model and the NCEP net surface heat flux fields adopted to drive the model simulation are fairly realistic. Similarly as the sea level comparison, misfit between observed and simulated SST also

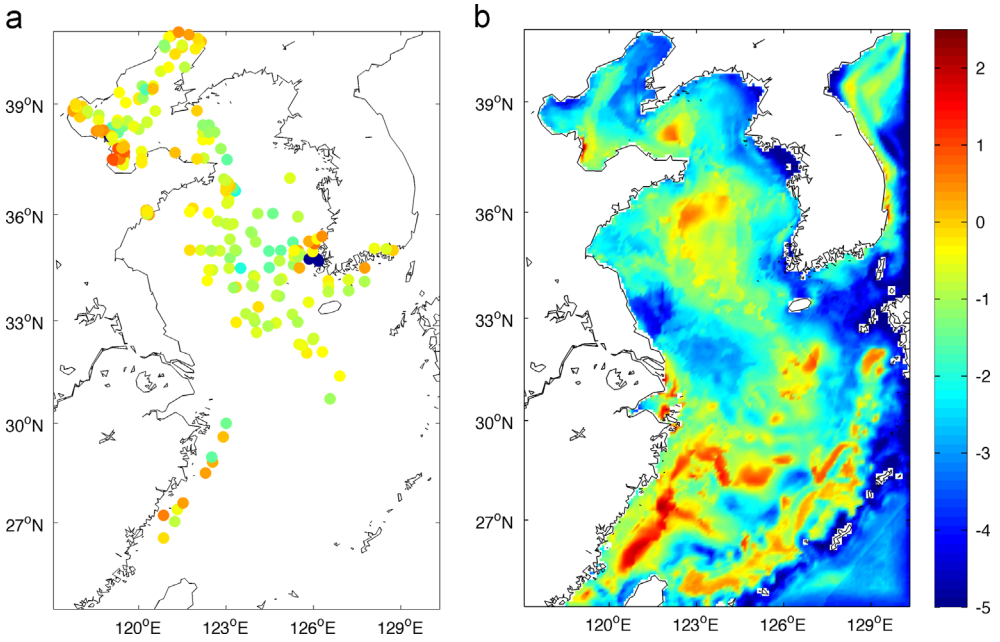

Fig. 4. Sediment accumulation rate comparison of (a) observations and (b) model output (temporal mean of 40 year time period: 1966–2005) (log10 cm/year).

occasionally occurs in peaks and troughs.

To further validate the model's skill in resolving the subsurface hydrographic features, we compared the temperature and salinity observations with the model output along the PN transect (Fig. 3c) in the ECS. Oceanographic data along the PN transect (see Fig. 1a for location) are available since 1960s, and have been extensively used to investigate the Kuroshio in the ECS (e.g., Lü et al., 2004). For our purpose, we computed long-term monthly averages (Wang, 2009) from model output and observations, and compared the salient temperature and salinity features in each month. Modeled and observed fields closely resemble each other. For instance, in January, the KC can be easily identified as the region of high temperature and salinity off the shelf slope. Temperature on the shelf is 5–6 °C colder, resulting in a strong temperature front at the shelf break (Fig. 3c). In July, SST rises up to 30 °C in both observation and model. Strong thermal stratification is seen in both, although the model results suggest a stronger upwelling and onshore transport. Both observation and model show a thin layer of fresh water (with salinity as low as 32.5) extending from the coast to the shelf break in the summer. This is due to the freshwater input from the Changjiang River and offshore transport caused by the southwest monsoon.

For the sediment model validation, we collected all available published accumulation rate data inside the study area (Fig. 4a). Because the model considered only the Huanghe and Changjiang River-derived sediment input and assumed there was no sediment on the seabed to begin with, we took the first eight years (1958–1965) as the sediment model spin-up period and let the modeled sediment field reach a quasi-steady state. Fig. 4b shows the modeled mean sediment accumulation rate averaged from 1966 to 2005 (the following analyses are all based on the same period unless explicitly indicated). Although the modeled sediment accumulation rate was generally less than observed likely due to the initialization from zero and not resolving some of the nearshore hydrodynamic process by our current model resolution), many observed features are reasonably well reproduced by the model. For instance, the accumulation rate, as seen in observations and model results, was larger at the muddy patches than other areas. When comparing the simulated accumulation rate (Fig. 4b) with the sediment grain size distribution (Fig. 1b), we can clearly see that the areas of high accumulation rate correspond to the fine-grain sediment areas (muddy patches). This is especially true for the muddy patches northeast of Shandong Peninsula in the northern YS, the YS Trough in the southern YS, south of Cheju Island, off the Zhejiang–Fujian coast, and along the Okinawa Trough. One model deficiency we have identified is that the model overpredicted the accumulation rate off the Zhejiang–Fujian coast. The mismatch is attributed to the weak Taiwan Warm Current in the model, and will be further discussed in the following sections.

3.2. *Seasonal variation of river-derived sediment transport in the BYECS*

Model-simulated depth-averaged current patterns show clear seasonal variations in ocean transport in the BYECS, in part due to seasonal changes of monsoon forcing (Fig. 5). For instance, in January the strong YSWC enters the middle southern YS, joins the southward KCC and forms a large clockwise gyre. The KCC and Tsushima Current (TC) pass through the Tsushima Strait with a weaker velocity. Along the Subei coast, the coastal currents flow southward, and further intensify south of the Changjiang River mouth. The Taiwan Warm Current (TWC) near Taiwan Island flows northward even under the strong northeastern monsoon. Further offshore, the strong KC enters the study area east of Taiwan Island, and exists south of Japan. While flowing mainly along the shelf break in the ECS, the KC northward intrusion occurs northeast of Taiwan Island, around 28.5 °N. In spring (April), the YSWC and coastal currents of the YS and ECS all become weaker. Because the northeast monsoon is diminishing, the TWC increases its strength. The KC intrusion and its exchange with continental shelf waters are still evident. In summer (July), the strength of YSWC further decreases, and the KCC flows northward along the west coast of the Korean Peninsula. Both the YSCC and ECSCC change their directions to the north. The ECSCC and TWC merge, forming a strong northward current along the Zhejiang–Fujian coast. In fall (October), the northward YSWC starts to strengthen, and the KCC changes its direction to the south again. The coastal currents along the Subei and Zhejiang–Fujian coast begin to flow southward,

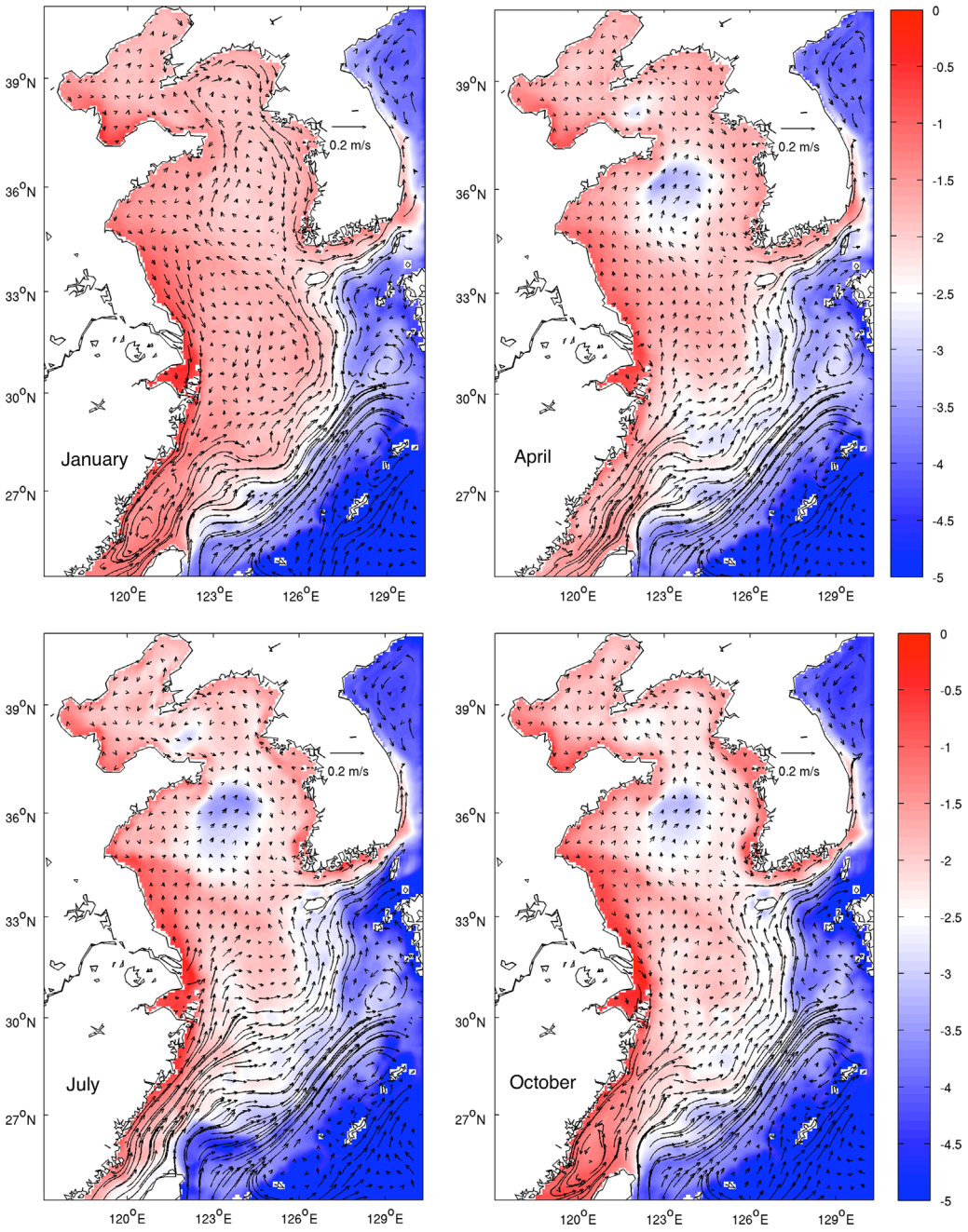

Fig. 5. Monthly depth-averaged current (arrows) and suspended sediment concentration (color, unit: log10 kg/m^3). Model output was temporally averaged from 1966 to 2005.

while the TWC starts to diminish. The KC's speed and direction are stable compared to other currents in the study area.

The depth-averaged suspended sediment concentration (SSC) also presents a clear seasonal variation (Fig. 5). The SSC over the continental shelf is the highest in winter (January). High SSC is seen near the Huanghe and Changjiang estuaries and nearby coasts, as expected near these sediment sources. In spring (April), the SSC over the continental shelf tapers, especially in the YS and ECS. Two interesting low SSC zones form, one in the YS, and the other near the entrance of the BS. Both correspond to locations of two muddy patches. In summer (July), the SSC near the Changjiang estuary further increases, but the SSC further offshore is reduced significantly when compared to that in the other seasons. Most of these spatial patterns remain the same in fall (October), with the SSC higher overall compared to summer. Note that, this pattern is quite similar to the field survey results of Dong et al. (2011) and Bian et al. (2013b), which show high surface SSC in winter, and low surface SSC in summer. Overall, high SSC occurs at the estuaries and coastal areas, while low SSC occurs in areas deeper than 100 m. The SSC over the continental shelf is higher in winter and lower in summer (Fig. 5), indicating that the sediment transport from coast to the shelf mainly happens in winter (Fig. 6). We can also see high SSC near the estuaries and nearby coast in summer (July), but low sediment flux over continental shelf (Fig. 6), suggesting that the river-derived sediment is mainly stored in these areas during summer in the form of suspended or temporarily

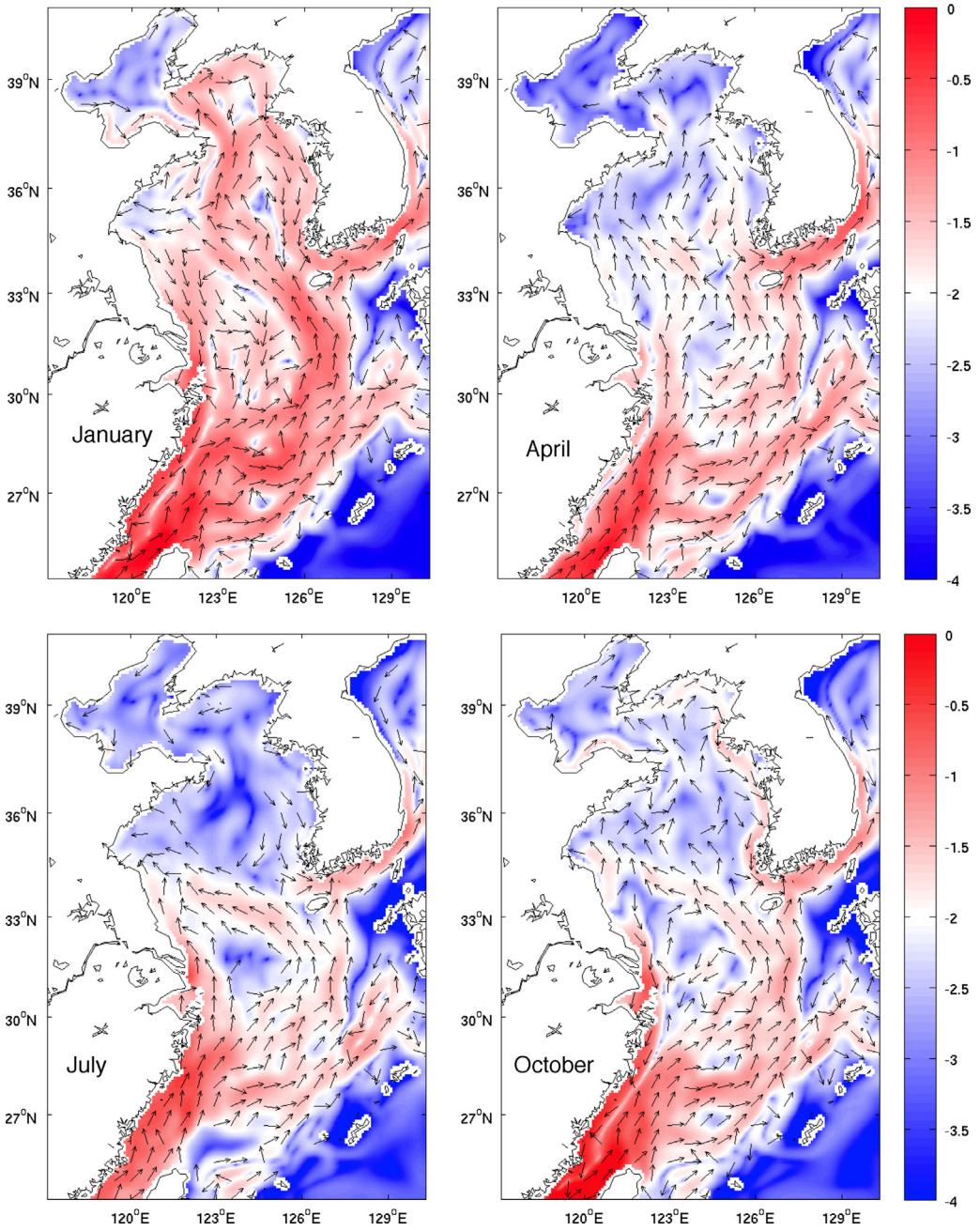

Fig. 6. Depth-integrated monthly mean sediment flux in the BYECS. Flux direction shown as arrows where flux exceeds 0.003 kg/(m s). The color scale is in log10 (unit: log10 kg/(m s)). Model output was temporally averaged from 1996 to 2005.

deposited sediment. This seasonal variation is similar to the field survey results of Bian et al. (2013b) and consistent with previous studies of sediment transport pattern in the BYECS (Yang et al., 1992; Yanagi et al., 1996; Sun et al., 2000).

To further verify the sediment transport pattern, we calculated the depth-integrated sediment flux of four months using the following equation (Harris et al., 2008):

$$\vec{F} = \int_0^H C\vec{U}\, dh$$

where $\vec{F}$ is the depth-integrated sediment flux, C is the monthly mean sediment concentration, $\vec{U}$ is the monthly mean current velocity, and H is the water depth. As expected, the sediment transport patterns also vary by season (Fig. 6). In winter (January), the YSCC along the Subei coast brings coastal sediment to the ECS continental shelf. Sediment along the Subei and Zhejiang–Fujian coast is transported southward, and meets with the TWC at the Taiwan Strait. The resulting convergent flows move riverine sediment to the outer shelf, where a bifurcation occurs. One branch of this sediment moves to the Okinawa Trough, the other branch travels north, joins the YSWC to the northern YS, and then joins with the KCC to swing around to the Tsushima Strait. In spring (April), the southward coastal sediment transport along the Zhejiang–Fujian coast shuts down. Instead, the sediment travels northward along the Chinese coast. Both the cross-shelf sediment transport and the YS flux gyre are significantly reduced as well. In summer (July), nearly all the coastal sediment along the Subei and

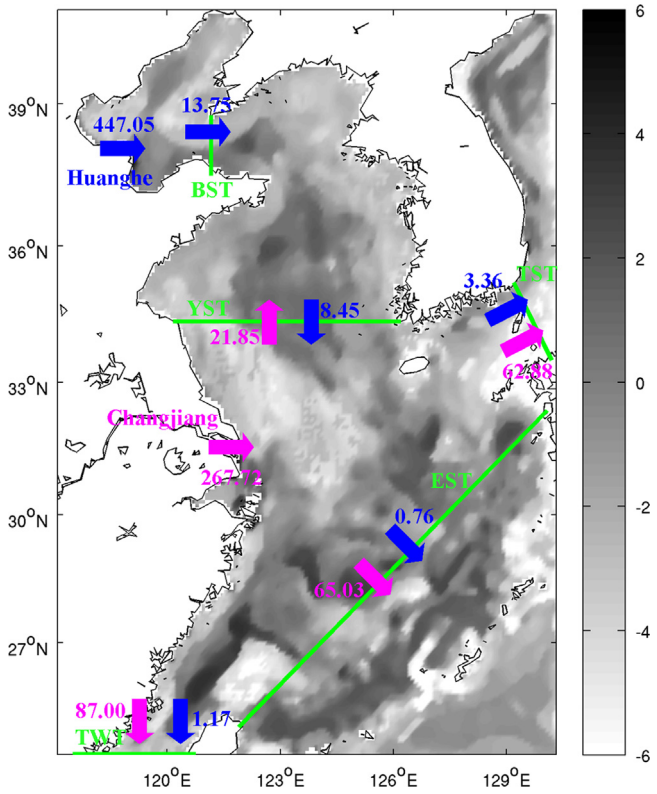

Fig. 7. Model-simulated sediment mass on the seabed in the last year of simulation (gray scale; log10 kg/m^2), and annual mean (1966–2005) sediment transport directions and amounts (mT/yr). Blue arrows and numbers represent Huanghe River sediment, while magenta arrows and numbers represent Changjiang River sediment. Flux values are from Table 2. Green lines are transects. BST: Bohai Sea transect; YST: Yellow Sea transect; TST: Tsushima Strait transect; EST: East China Sea transect; TWT: Taiwan Strait transect. (For interpretation of the references to color in this figure legend, the reader is referred to the web version of this article.)

Zhejiang–Fujian coast is transported northward. Although a portion of cross-shelf sediment transport can still reach the Okinawa Trough due to the TWC, the strength of sediment transport is reduced compared to its spring condition. In fall (October), the sediment flux near the Zhejiang–Fujian coast and Taiwan Strait increases. The sediment transport pattern tends to develop toward that of winter. The coastal sediment travels southward again along the Subei and Zhejiang–Fujian coast, and the cross-shelf transport picks up again. Overall, our model results show that the largest (least) sediment flux is present over the continental shelf in winter (summer). Likewise, stronger (weaker) offshore sediment transport occurs in winter (summer). Because our model's southern open boundary cuts across the TWC, its ability to resolve the variability of TWC is largely dependent on the quality of SODA model fields that provide boundary values for our model. Further refinement of TWC simulation and investigation of its impact on cross-shelf sediment transport will be carried out in a future study.

To further quantify sediment transport, we calculated the long-term (1966–2005) mean sediment (in million tons) transported across several transects in the study domain (Fig. 7). Most of the Huanghe-derived sediment (447.05 mT/yr) stays within the BS, with only 3% (13.75 mT/yr) traveling into the YS. Within this portion, 1.17 mT/yr subsequently passed the Taiwan Strait into the South China Sea, 3.36 mT/yr was exported at the Tsushima Strait, and only 0.76 mT/yr reached the Okinawa Trough. The mean Changjiang-derived sediment totaled 267.72 mT/yr, of which 8% (21.85 mT/yr) entered the YS, 32% (87.00 mT/yr) passed the Taiwan

Table 2
Temporally averaged (1966–2005) river-derived sediment (million tons) moving across transects in Fig. 7. (a) Huanghe River sediment; (b) Changjiang River sediment. Directions are shown in Fig. 7. BST: Bohai Sea transect; YST: Yellow Sea transect; TST: Tsushima Strait transect; EST: East China Sea transect; TWT: Taiwan Strait transect.

(a) Huanghe	Input	BST	YST	EST	TST	TWT
Spring	25.38	0.92	1.18	0.25	1.18	0.02
Summer	209.04	0.83	0.03	0.12	0.20	0.00
Fall	203.17	5.00	1.90	0.11	0.79	0.83
Winter	9.46	7.01	5.34	0.28	1.18	0.31
Annual	447.05	13.75	8.45	0.76	3.36	1.17

(b) Changjiang	Input	YST	EST	TST	TWT
Spring	32.57	7.18	22.70	22.16	2.43
Summer	137.66	5.19	11.26	5.68	0.00
Fall	85.92	4.00	10.17	19.15	49.28
Winter	11.57	5.48	20.90	15.89	35.28
Annual	267.72	21.85	65.03	62.88	87.00

Strait, and ~24% (65.03 and 62.88 mT/yr, respectively) each reached the Okinawa Trough and Tsushima Strait. The remaining 12% settled on the ECS continental shelf. Note that, because we only considered two classes sediment, and some sediment processes (e.g. flocculation) are not included in the model, the sediment transport across those transects may be overestimated.

Long-term averages of river-derived sediment show strong seasonal variation. The largest input of Huanghe sediment occurs in summer and fall (Table 2). The outward sediment transport across the BS transect (BST), YS transect (YST), and Taiwan transect

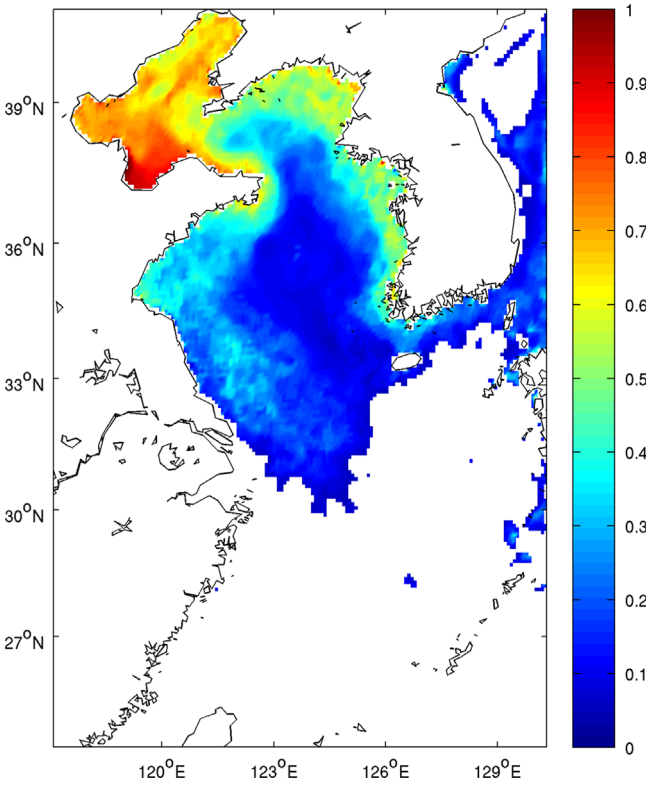

Fig. 8. Fraction of Huanghe River-derived sediment on the seabed in the last model year (only areas > 0.05 are shown). Changjiang River-derived sediment fraction can be calculated as 1 -fraction of Huanghe sediment.

(TWT) is greatest in fall and winter. Note that because we did not consider any sediment input through the open boundaries, only the outward sediment transport across the TWT was counted in Table 2. It is probable that the sediment transported across the Taiwan Strait transect may be brought back by the northward current in summer. For the ECS transect (EST) and Tsushima Strait transect (TST), winter and spring transport are larger than other seasons. The largest input of Changjiang sediment also occurs in summer and fall. The northward transport of Changjing sediment across the YS transect does not have obvious seasonal variation. Similar to the Huanghe sediment, the transport of Changjiang sediment to the Okinawa Trough mainly occurred in spring and winter. Less Changjiang sediment crossed the Tsushima Strait transect in summer. The southward transport of Changjiang sediment dominates in fall and winter for the Taiwan transect. Subject to the open boundary specifications along the Taiwan Strait, the sediment flux across the TWT may need further refinement.

The model-simulated sediment distribution (Fig. 7) in the last model year (2005) corresponds well with observed muddy patch data (Fig. 1b), which are also high-accumulation-rate regions. The location of two muddy patches in the YS, the muddy patches along the Zhejiang–Fujian coast, south of Cheju Island, and along the Okinawa Trough are all reproduced by the model. Due to the uncertainty associated with SODA model data along the southern boundary across the Taiwan Strait, the strength of the TWC may have been underestimated in our model, which would lead to more sediment being transported to the outer shelf and farther to the Okinawa Trough. As a result, the estimated accumulation rate and sediment mass are probably higher than the actual values in those regions. The spatial distribution of seabed sediment fraction (Huanghe-derived vs. Changjiang-derived) indicates Huanghe-derived sediment dominates the BS, while Changjiang-derived sediment dominates the ECS and most of the YS (Fig. 8, Table 2). Outward transport of the Huanghe sediment mainly occurred along the Shandong and Korean Peninsula coasts.

3.3. Seasonal variation of bottom stress in the BYECS

Bottom stress is known to be a very important parameter for sediment transport (Warner et al., 2008b). When bottom stress is larger (smaller) than the critical shear stress of sediment, suspension (deposition) occurs (Warner et al., 2008b, 2010). This combines with transport by background currents and wave actions, causing the river-derived sediment to be transported farther away from river mouths. To better understand the sediment transport mechanism in the BYECS, we examined the long-term mean bottom stress induced by waves (τ_w), currents (τ_c), and wave–current combined (τ_t) (Fig. 9). The wave-induced bottom stress (Fig. 9a) is greater near the coasts than in deep water. The maximum values are located along the Subei and Zhejiang–Fujian coast. Current-induced bottom stress has a more complex spatial pattern (Fig. 9b), and plays a more important role in determining the combined bottom stress distribution over the continental shelf. Areas with higher accumulation rates (Fig. 4) are also the regions with large sediment mass on seabed (Fig. 7) and weaker bottom stress (Fig. 9c), which also generally correspond to the muddy patches (Fig. 1b). Weak bottom stress is associated with low-energy near bottom, where sediment tends to deposit in these regions. More sediment deposition implies higher accumulation rates. Because these regions are generally far from river mouths, most sediment carried there is fine sediment with small grain size. These weak bottom stress regions serve like “sediment traps” in the study area. The “tongue” of high bottom stress across the ECS shelf (Fig. 9b and c) indicates that sediment in this area is more likely to be transported away than to settle locally. Although bottom stress is large at the two river mouths (Fig. 9c), the accumulation of sediment in those areas is still significant, mainly due to their proximity to the river mouths and thus the sediment sources.

We further explored the seasonal variations of wave-induced, current-induced, and wave–current combined bottom stress anomaly relative to corresponding long-term means (Fig. 10). Wave-induced bottom stress has a pronounced seasonal variation, being largest in winter (January), and smallest in summer (July) (Fig. 10a) due to the influence of monsoon. The variation of current-induced bottom stress is small. The largest current-induced bottom stress occurs near the Subei coast and in the YS in winter (January) (Fig. 10b). As a result, the combined bottom stress (τ_t) near the coast is largest in winter (January), and smallest in summer (July) (Fig. 10c).

In winter, erosion/suspension associated with strong combined bottom stress along the northern Shandong Peninsula makes it possible for Huanghe sediment to move from the BS to the YS. Similarly, the large combined bottom stress near the Subei and

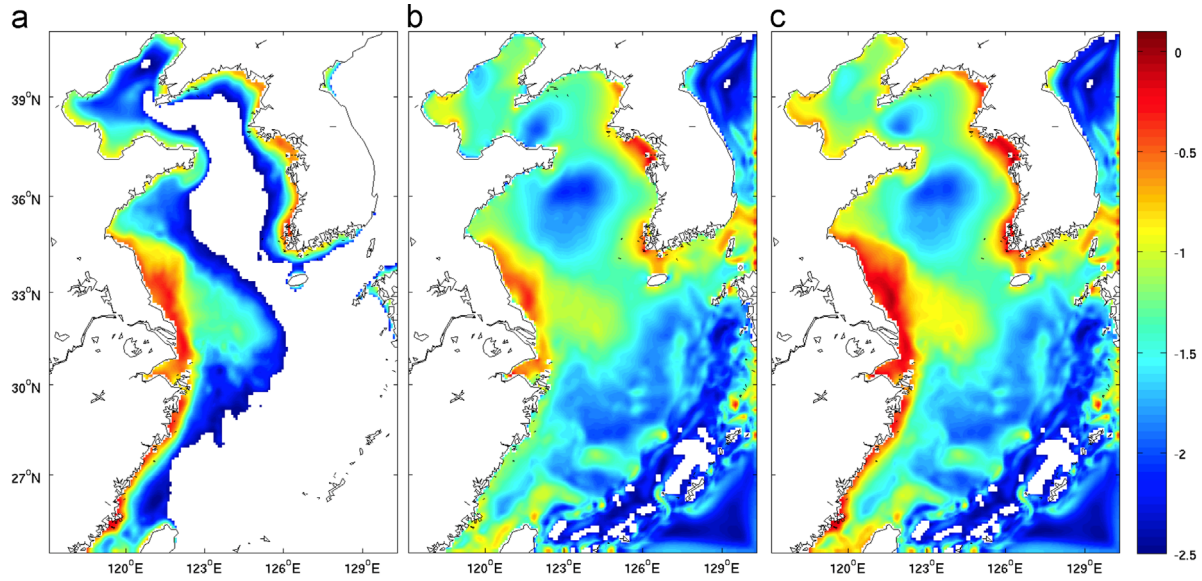

Fig. 9. Long-term (1966–2005) mean bottom stress (log10 N/m^2). (a) Wave-induced; (b) current-induced; (c) wave–current combined. Only values > 0.003 N/m^2 were plotted.

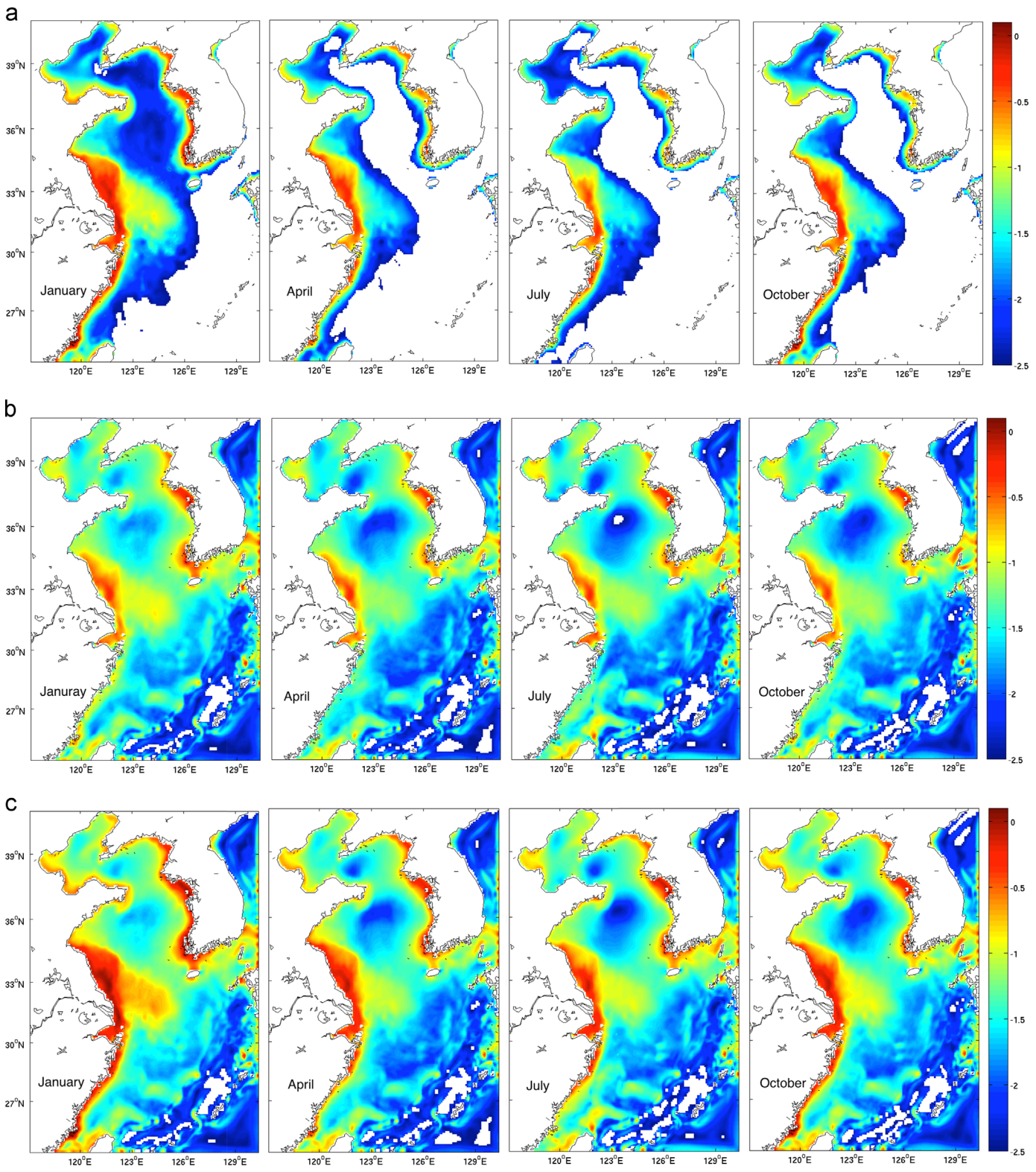

Fig. 10. Monthly mean bottom stress anomaly in January, April, July, and October. (a) Wave-induced; (b) current-induced; (c) wave–current combined. Model output was temporally averaged from 1996 to 2005.

Zhejiang–Fujian coasts allows suspension, and further facilitates the southward transport of Changjiang sediment. The high combined bottom stress tongue from the Subei coast to the Okinawa Trough in winter also implies this is likely the pathway for cross-shelf sediment transport in winter. In summer (July), bottom stress along the northern Shandong Peninsula is the weakest among the four seasons, corresponding to the least outward transport of suspended Huanghe sediment. The high bottom stress tongue toward the Okinawa Trough also shrinks in July, implying less-effective cross-shelf sediment transport in this season. At the same time, weak combined bottom stress near the Zhejiang–Fujian coast suspends less sediment, preventing sediment from being

transported away from the inner shelf to the deep ocean.

4. Summary

The wave–current–sediment coupled model was used to study the coastal circulation and transport of Huanghe and Changjiang River-derived sediment in the Bohai, Yellow, and East China Seas (BYECS) over the past several decades. Model validations against wave and hydrographical observations demonstrated that the model can reasonably well reproduce the hydrodynamic environment of the BYECS. Model-simulated high-accumulation rate regions correspond with observed fine sediment areas (muddy patches; Fig. 1b). The formation of muddy patches near river mouths is mainly due to their proximity to the sediment input source. Muddy patches formed in regions farther away from river mouths are results of weak bottom stress and related circulation patterns (Fig. 9). Model-simulated seabed sediment distribution shows that most of the Huanghe sediment load is confined in the BS and settles near northern Shandong Peninsula (Fig. 8). Two major export pathways are identified for Huanghe sediment: one along the Shandong Peninsula coast, and the other along the west Korean coast. Changjiang sediment spreads over the entire ECS and beyond, including a branch extending into the YS via the YSWC.

The river-derived sediment transport in the BYECS has very strong seasonal variation (Fig. 6). Generally, sediment tends to be transported away in winter, and stays near the estuaries in summer. For Huanghe-derived sediment, erosion (suspension) and export along the Shandong Peninsula are mainly controlled by wave-induced bottom stress, which is strong in winter and weak in summer. For Changjiang-derived sediment, both wave-induced and current-induced bottom stresses are important. Stronger bottom stress allows more active seabed erosion and suspension of seabed sediment, allowing sediment to be carried away by the coastal current. In summer and as a result of the southwest monsoon, the coastal current along the Zhejiang–Fujian coast flows northward, blocking southward sediment transport and preventing the sediment from escaping from the inner shelf. Sediment traps (e.g. Hsu et al., 2004) could be designed in this area to further verify this seasonal variation. It is possible that this seasonal variation of sediment transport may also exist in other monsoon influenced coastal regions. The river-derived sediment distribution, to some extent, may also reflect the distribution pattern of anthropogenic contaminants in the ocean, which affect the regional marine ecosystem (e.g. Zhang, 1999; Qiao et al., 2007).

To simplify our analyses, we only considered wave, current, sediment coupling, and two rivers' sediment input in this study. In reality, the sediment that was deposited on seabed and biological activities can also affect the sediment accumulation and transport patterns. A future effort may also consider the coupling with the atmosphere, and examine more complex sediment transport dynamics during major storms. This modeling system can potentially be used in other coastal regions. More accurate specifications of open boundary conditions and mixing parameterizations used in both hydrodynamic and sediment transport processes can also help to improve model capability in studying coastal sediment dynamics.

Acknowledgments

Research support provided by U.S. Geological Survey Coastal Process Project and Chinese National Key Fundamental Research Grant 2014CB745004 is much appreciated. We also thank three anonymous reviewers for their constructive comments.

Appendix A. List of abbreviations

Abbreviation	Full name
BYECS	Bohai, Yellow, and East China Seas
BS	Bohai Sea
YS	Yellow Sea
ECS	East China Sea
YSWC	Yellow Sea Warm Current
YSCC	Yellow Sea Coastal Current
KCC	Korean Coastal Current
ECSCC	East China Sea Coastal Current
KC	Kuroshio Current
TC	Tsushima Current
TWC	Taiwan Warm Current
BST	Bohai Sea transect
YST	Yellow Sea transect
TWT	Taiwan transect
EST	East China Sea transect
TST	Tsushima Strait transect

References

Bever, A.J., Harris, C.K., Sherwood, C.R., Signell, R.P., 2009. Deposition and flux of sediment from the Po River Italy: an idealized and wintertime numerical modeling study. Mar. Geol. 260; , pp. 69–80. http://dx.doi.org/10.1016/j.margeo.2009.01.007.

Bian, C., Jiang, W., Greatbatch, R.J., 2013a. An exploratory model study of sediment transport sources and deposits in the Bohai Sea, Yellow Sea and East China Sea. J. Geophys. Res.: Oceans 118, 5908–5923. http://dx.doi.org/10.1002/2013JC009116.

Bian, C., Jiang, W., Quan, Q., Wang, T., Greatbatch, R.J., Li, W., 2013b. Distributions of suspended sediment concentration in the Yellow Sea and the East China Sea

based on field surveys during the four seasons of 2011. J. Mar. Syst. 121–122, 24–35. http://dx.doi.org/10.1016/j.jmarsys.2013.03.013.
Bonaldo, D., Di Silvio, G., 2013. Historical evolution of a micro-tidal lagoon simulated by a 2-D schematic model. Geomorphology 201, 380–396. http://dx.doi.org/10.1016/j.geomorph.2013.07.012.
Booij, N., Ris, R.C., Holthuijsen, L.H., 1999. A third-generation wave model for coastal regions: 1. Model description and validation. J. Geophys. Res. 104, 7649–7666. http://dx.doi.org/10.1029/98JC02622.
Carton, J.A., Chepurin, G., Cao, X., 2000a. A simple ocean data assimilation analysis of the global upper ocean 1950–95. Part II: Results. J. Phys. Oceanogr. 30, 311–326 10.1175/1520-0485(2000)030 < 0311:ASODAA > 2.0.CO;2.
Carton, J.A., Chepurin, G., Cao, X., Giese, B., 2000b. A simple ocean data assimilation analysis of the global upper ocean 1950–95. Part I: Methodology. J. Phys. Oceanogr. 30, 294–309. http://dx.doi.org/10.1175/1520-0485(2000)030 < 0294:ASODAA > 2.0.CO;2.
Choi, B.H., 1983. Sediment transport paths in the East China Sea. J. Korean Soc. Civ. Eng. 3, 83–93.
DeMaster, D.J., McKee, B.A., Nittrouer, C.A., Jiangchu, Q., Guodong, C., 1985. Rates of sediment accumulation and particle reworking based on radiochemical measurements from continental shelf deposits in the East China Sea. Cont. Shelf Res. 4, 143–158. http://dx.doi.org/10.1016/0278-4343(85)90026-3.
Deng, J.Y., Yang, C.H., 1993. Marine fishery. In: Tseng, C.K., Zhou, H.O., Li, B.C. (Eds.), Marine Science Study and its Prospect in China. Qingdao Publishing House, Qingdao, China, pp. 681–688.
Dong, L.X., Su, J.L., Wang, K.S., 1989. Tide current in the Yellow Sea and its relationship with sediment transport. Acta Oceanol. Sin. 11, 102–114.
Dong, L.X., Guan, W.B., Chen, Q., Li, X.H., Liu, X.H., Zeng, X.M., 2011. Sediment transport in the Yellow Sea and East China Sea. Estuar. Coast. Shelf Sci. 93, 248–258. http://dx.doi.org/10.1016/j.ecss.2011.04.003.
Egbert, G.D., Bennett, A.F., Foreman, M.G.G., 1994. TOPEX/POSEIDON tides estimated using a global inverse model. J. Geophys. Res. 99, 24821–24852. http://dx.doi.org/10.1029/94JC01894.
Egbert, G.D., Erofeeva, S.Y., 2002. Efficient inverse modeling of barotropic ocean tides. J. Atmos. Ocean. Technol. 19, 183–204. http://dx.doi.org/10.1175/1520-0426(2002)019 < 0183:EIMOBO > 2.0.CO;2.
Emery, K.O., 1968. Relict sediments on continental shelves of world. AAPG Bull. 52 (3), 445–464.
Guan, B., 1994. Patterns and structures of the currents in Bohai, Huanghai and East China Seas. In: Di, Z., Yuan-Bo, L., Tseng, Z.C.-K.C.K. (Eds.), Oceanology of China Seas. Springer, Netherlands, pp. 17–26.
Haidvogel, D.B., Arango, H., Budgell, W.P., Cornuelle, B.D., Curchitser, E., Di Lorenzo, E., Fennel, K., Geyer, W.R., Hermann, A.J., Lanerolle, L., Levin, J., McWilliams, J.C., Miller, A.J., Moore, A.M., Powell, T.M., Shchepetkin, A.F., Sherwood, C.R., Signell, R.P., Warner, J.C., Wilkin, J., 2008. Ocean forecasting in terrain-following coordinates: formulation and skill assessment of the Regional Ocean Modeling System. J. Comput. Phys. Predict. Weather Clim. Extreme Events 227, 3595–3624. http://dx.doi.org/10.1016/j.jcp.2007.06.016.
Harris, C.K., Sherwood, C.R., Signell, R.P., Bever, A.J., Warner, J.C., 2008. Sediment dispersal in the northwestern Adriatic Sea. J. Geophys. Res.: Oceans 113, C11S03. http://dx.doi.org/10.1029/2006JC003868.
Hsu, S.-C., Lin, F.-J., Jeng, W.-L., Chung, Y., Shaw, L.-M., Hung, K.-W., 2004. Observed sediment fluxes in the southwesternmost Okinawa Trough enhanced by episodic events: flood runoff from Taiwan rivers and large earthquakes. Deep Sea Res. Part I: Oceanogr. Res. Pap. 51, 979–997. http://dx.doi.org/10.1016/j.dsr.2004.01.009.
Hu, D.X., Han, W.Y., Zhang, S., 2001. Land–Ocean Interactions in the Yangtze and Pearl Estuaries and the their Adjacent Waters. China Ocean Press, Beijing, pp. 58–89.
Hu, L.M., Lin, T., Shi, X.F., Yang, Z.S., Wang, H.J., Zhang, G., Guo, Z.G., 2011. The role of shelf mud depositional process and large river inputs on the fate of organochlorine pesticides in sediments of the Yellow and East China seas. Geophys. Res. Lett. 38, L03602. http://dx.doi.org/10.1029/2010GL045723.
Huang, D., Su, J., Backhaus, J.O., 1999. Modelling the seasonal thermal stratification and baroclinic circulation in the Bohai Sea. Cont. Shelf Res. 19, 1485–1505. http://dx.doi.org/10.1016/S0278-4343(99)00026-6.
Ichikawa, H., Beardsley, R.C., 2002. The current system in the Yellow and East China Seas. J. Oceanogr. 58, 77–92. http://dx.doi.org/10.1023/A:1015876701363.
Jiang, W., Pohlmann, T., Sündermann, J., Feng, S., 2000. A modelling study of SPM transport in the Bohai Sea. J. Mar. Syst. 24, 175–200. http://dx.doi.org/10.1016/S0924-7963(99)00071-8.
Jiang, W., Pohlmann, T., Sun, J., Starke, A., 2004. SPM transport in the Bohai Sea: field experiments and numerical modelling. J. Mar. Syst. 44, 175–188. http://dx.doi.org/10.1016/j.jmarsys.2003.09.009.
Kalnay, E., Kanamitsu, M., Kistler, R., Collins, W., Deaven, D., Gandin, L., Iredell, M., Saha, S., White, G., Woollen, J., Zhu, Y., Leetmaa, A., Reynolds, R., Chelliah, M., Ebisuzaki, W., Higgins, W., Janowiak, J., Mo, K.C., Ropelewski, C., Wang, J., Jenne, Roy, Joseph, Dennis, 1996. The NCEP/NCAR 40-year reanalysis project. Bull. Am. Meteor. Soc. 77, 437–471. http://dx.doi.org/10.1175/1520-0477(1996)077 < 0437:TNYRP > 2.0.CO;2.
Kumar, N., Voulgaris, G., Warner, J.C., Olabarrieta, M., 2012. Implementation of the vortex force formalism in the coupled ocean-atmosphere-wave-sediment transport (COAWST) modeling system for inner shelf and surf zone applications. Ocean Model. 47, 65–95.
Larson, J., Jacob, R., Ong, E., 2005. The model coupling toolkit: a new Fortran90 toolkit for building multiphysics parallel coupled models. Int. J. High Perform. Comput. Appl. 19, 277–292. http://dx.doi.org/10.1177/1094342005056115.
Li, G., Yang, Z., Liu, Y., 2005a. Formation Environment of the Seafloor Sediment in the East China Seas. Science Press, Beijing, pp. 45–49.
Li, G., Wang, H., Liao, H., 2005b. Numerical simulation on seasonal transport variations and mechanisms of suspended sediment discharged from the Yellow River to the Bohai Sea. Acta Geogr. Sin. 60, 707–716.
Li, J.B., 2008. Regional Geology in East China Sea. Ocean Press, Beijing, p. 631.
Lie, H.J., 1986. Summertime hydrographic feature in the southeastern Huanghe. Prog. Oceanogr. 17, 229–242.
Lin, S., Hsieh, I.-J., Huang, K.-M., Wang, C.-H., 2002. Influence of the Yangtze River and grain size on the spatial variations of heavy metals and organic carbon in the East China Sea continental shelf sediments. Chem. Geol. 182, 377–394. http://dx.doi.org/10.1016/S0009-2541(01)00331-X.
Liu, C., Sui, J., He, Y., Hirshfield, F., 2013. Changes in runoff and sediment load from major Chinese rivers to the Pacific Ocean over the period 1955–2010. Int. J. Sediment Res. 28, 486–495. http://dx.doi.org/10.1016/S1001-6279(14)60007-X.
Liu, J.P., Milliman, J.D., Gao, S., 2002. The Shandong mud wedge and post-glacial sediment accumulation in the Yellow Sea. Geo-Mar. Lett. 21, 212–218. http://dx.doi.org/10.1007/s00367-001-0083-5.
Liu, J.P., Li, A.C., Xu, K.H., Velozzi, D.M., Yang, Z.S., Milliman, J.D., DeMaster, D.J., 2006. Sedimentary features of the Yangtze River-derived along-shelf clinoform deposit in the East China Sea. Cont. Shelf Res. 26, 2141–2156. http://dx.doi.org/10.1016/j.csr.2006.07.013, Special Issue in Honor of Richard W. Sternberg's Contributions to Marine Sedimentology.
Liu, J.P., Xu, K.H., Li, A.C., Milliman, J.D., Velozzi, D.M., Xiao, S.B., Yang, Z.S., 2007. Flux and fate of Yangtze River sediment delivered to the East China Sea. Geomorphol. Monsoon Rivers Asia 85, 208–224. http://dx.doi.org/10.1016/j.geomorph.2006.03.023.
Liu, J., Xue, Z., Ross, K., Wang, H., Yang, Z., Li, A., Gao, S., 2009. Fate of sediments delivered to the sea by Asian large rivers: long-distance transport and formation of remote alongshore clinothems. Sediment. Rec. 7, 4.
Lu, J., Qiao, F.L., Wang, X.H., Wang, Y.G., Teng, Y., Xia, C.S., 2011. A numerical study of transport dynamics and seasonal variability of the Yellow River sediment in the Bohai and Yellow seas. Estuar. Coast. Shelf Sci. 95, 39–51. http://dx.doi.org/10.1016/j.ecss.2011.08.001.
Lü, L.-G., Chen, H.-X., Yuan, Y.-L., 2004. Spatial and temporal variations of sound speed at the PN section. J. Oceanogr. 60, 673–679. http://dx.doi.org/10.1007/s10872-004-5760-3.
Ma, M., Feng, Z., Guan, C., Ma, Y., Xu, H., Li, H., 2001. DDT, PAH and PCB in Sediments from the Intertidal Zone of the Bohai Sea and the Yellow Sea. Mar. Pollut. Bull. 42, 132–136. http://dx.doi.org/10.1016/S0025-326X(00)00118-1.
Madsen, O., 1994. Spectral wave–current bottom boundary layer flows. Coast. Eng. Proc. 1 (24), 384–398. http://dx.doi.org/10.9753/icce.v24.%p.
Mellor, G.L., Yamada, T., 1982. Development of a turbulence closure model for geophysical fluid problems. Rev. Geophys. 20, 851–875. http://dx.doi.org/10.1029/RG020i004p00851.
Milliman, J.D., Meade, R.H., 1983. World-wide delivery of river sediment to the oceans. J. Geol. 91, 1–21.
Milliman, J.D., Beardsley, R.C., Zuo-sheng, Y., Limeburner, R., 1985a. Modern Huanghe-derived muds on the outer shelf of the East China Sea: identification and potential transport mechanisms. Cont. Shelf Res. Sediment Dyn. Changjiang Estuary Adjac. East China Sea 4, 175–188. http://dx.doi.org/10.1016/0278–4343(85)90028-7.
Milliman, J.D., Shen, H.-T., Yang, Z.-S., Mead, R.H., 1985b. Transport and deposition of river sediment in the Changjiang estuary and adjacent continental shelf. Cont. Shelf Res. Sediment Dyn. Changjiang Estuary Adjac. East China Sea 4, 37–45. http://dx.doi.org/10.1016/0278–4343(85)90020-2.
Milliman, J.D., Yang, Z., 2014. Chinese-U.S. sediment source-to-sink research in the east China and Yellow Seas: a brief history. Cont. Shelf Res. Sediment Dyn. Changjiang Estuary Adjac. East China Sea 90, 2–4. http://dx.doi.org/10.1016/j.csr.2014.09.008.
Naimie, C.E., Ann Blain, C., Lynch, D.R., 2001. Seasonal mean circulation in the Yellow Sea—a model-generated climatology. Cont. Shelf Res. 21, 667–695. http://dx.doi.org/10.1016/S0278-4343(00)00102-3.
National Geophysical Data Center, 2006. 2-minute Gridded Global Relief Data (ETOPO2) v2. National Geophysical Data Center, NOAA. doi:10.7289/V5J1012Q.
Olabarrieta, M., Warner, J.C., Kumar, N., 2011. Wave–current interaction in Willapa Bay. J. Geophys. Res. 116, C12014. http://dx.doi.org/10.1029/2011JC007387.
Orlanski, I., 1976. A simple boundary condition for unbounded hyperbolic flows. J. Comput. Phys. 21, 251–269. http://dx.doi.org/10.1016/0021–9991(76)90023-1.
Pan, Y., Su, J., Xu, D., 1987a. Oceanographic conditions of Taiwan Warm Current area during June–July 1984. Collection of Papers on Kuroshio Survey and Research, State Oceanic Administration of China. Ocean Publisher, Beijing, China, pp. 118–132.
Pan, Y., Su, J., Xu, D., 1987b. Oceanographic conditions of Taiwan Warm Current area during December 1984–January 1985. Collection of Papers on Kuroshio Survey and Research, State Oceanic Administration of China. Ocean Publisher, Beijing, China, pp. 149–162.
Park, Y.-H., 1986. Water characteristics and movements of the Yellow Sea Warm Current in summer. Prog. Oceanogr. 17, 243–254. http://dx.doi.org/10.1016/0079–6611(86)90047-9.
Qiao, S., Yang, Z., Pan, Y., Guo, Z., 2007. Metals in suspended sediments from the Changjiang (Yangtze River) and Huanghe (Yellow River) to the sea, and their comparison. Estuar. Coast. Shelf Sci. 74, 539–548. http://dx.doi.org/10.1016/j.ecss.2007.05.042.
Qin, Y., 1994. Sedimentation in Northern China Seas. In: Di, Z., Yuan-Bo, L., Cheng-Kui, Z. (Eds.), Oceanology of China Seas. Springer, Netherlands, pp. 395–406.

Saito, Y., Yang, Z., 1995. Historical change of the Huanghe (Yellow River) and its impact on the sediment budget of the East China Sea. In: Tsunogai, S. (Ed.), Proceedings of the 1994 Sapporo IGBP Symposium. Hokkaido University, Sapporo, Japan, pp. 7–12.

Sclavo, M., Benetazzo, A., Carniel, S., Bergamasco, A., Falcieri, F.M., Bonaldo, D., 2013. Wave-current interaction effect on sediment dispersal in a shallow semi-enclosed basin. J. Coast. Res. 65, 1587–1592. http://dx.doi.org/10.2112/SI65-268.1.

Shchepetkin, A.F., McWilliams, J.C., 2005. The regional oceanic modeling system (ROMS): a split-explicit, free-surface, topography-following-coordinate oceanic model. Ocean Model. 9, 347–404. http://dx.doi.org/10.1016/j.ocemod.2004.08.002.

Shchepetkin, A.F., McWilliams, J.C., 2009. Correction and commentary for "Ocean forecasting in terrain-following coordinates: formulation and skill assessment of the regional ocean modeling system" by Haidvogel et al. J. Comp. Phys. 227, 3595–3624, J. Comput. Phys. 228, 8985–9000. doi:10.1016/j.jcp.2009.09.002.

Su, J., 2001. A review of circulation dynamics of the coastal oceans near China. Acta Oceanolog. Sin. 23, 1–16.

Sun, X., Fang, M., Huang, W., 2000. Spatial and temporal variations in suspended particulate matter transport on the Yellow and East China Sea shelf. Oceanol. Limnol. Sin. 31, 581–587.

Wang, H., Wang, A., Bi, N., Zeng, X., Xiao, H., 2014. Seasonal distribution of suspended sediment in the Bohai Sea, China. Continental Shelf Research. Sediment Dyn. Relat. Biogeochem. Effects Eastern China Shelf Seas 90, 17–32. http://dx.doi.org/10.1016/j.csr.2014.03.006.

Wang, H., Yang, Z., Li, Y., Guo, Z., Sun, X., Wang, Y., 2007a. Dispersal pattern of suspended sediment in the shear frontal zone off the Huanghe (Yellow River) mouth. Cont. Shelf Res. 27, 854–871. http://dx.doi.org/10.1016/j.csr.2006.12.002.

Wang, X.H., Pinardi, N., Malacic, V., 2007b. Sediment transport and resuspension due to combined motion of wave and current in the northern Adriatic Sea during a Bora event in January 2001: a numerical modelling study. Cont. Shelf Res. 27, 613–633. http://dx.doi.org/10.1016/j.csr.2006.10.008.

Wang, Y., 2009. On the Simulation of the Long-term Change of the Physical Environment in East China Sea (PhD dissertation). Ocean University of China.

Warner, J.C., Sherwood, C.R., Arango, H.G., Signell, R.P., 2005. Performance of four turbulence closure models implemented using a generic length scale method. Ocean Model. 8, 81–113. http://dx.doi.org/10.1016/j.ocemod.2003.12.003.

Warner, J.C., Armstrong, B., He, R., Zambon, J.B., 2010. Development of a Coupled Ocean–Atmosphere–Wave–Sediment Transport (COAWST) Modeling System. Ocean Model. 35, 230–244. http://dx.doi.org/10.1016/j.ocemod.2010.07.010.

Warner, J.C., Butman, B., Dalyander, P.S., 2008a. Storm-driven sediment transport in Massachusetts Bay. Cont. Shelf Res. 28, 257–282. http://dx.doi.org/10.1016/j.csr.2007.08.008.

Warner, J.C., Sherwood, C.R., Signell, R.P., Harris, C.K., Arango, H.G., 2008b. Development of a three-dimensional, regional, coupled wave, current, and sediment-transport model. Comput. Geosci. 34, 1284–1306. http://dx.doi.org/10.1016/j.cageo.2008.02.012.

Wu, Y., Zhang, J., Mi, T., Li, B., 2001. Occurrence of n-alkanes and polycyclic aromatic hydrocarbons in the core sediments of the Yellow Sea. Mar. Chem. 76, 1–15. http://dx.doi.org/10.1016/S0304-4203(01)00040-8.

Xia, C., Qiao, F., Yang, Y., Ma, J., Yuan, Y., 2006. Three-dimensional structure of the summertime circulation in the Yellow Sea from a wave-tide-circulation coupled model. J. Geophys. Res. 111, C11S03. http://dx.doi.org/10.1029/2005JC003218.

Xiao, S.B., Li, A.C., Jiang, F.Q., You, Z., Chen, L., 2005. Provenance analysis of mud along the Min-Zhe coast since 2kaBP. Acta Sedimentol. Sin. 23 (2) 368–274.

Xue, Z., He, R., Liu, J.P., Warner, J.C., 2012. Modeling transport and deposition of the Mekong River sediment. Contin. Shelf Res. 37, 66–78. http://dx.doi.org/10.1016/j.csr.2012.02.010.

Xu, K., Harris, C.K., Hetland, R.D., Kaihatu, J.M., 2011. Dispersal of Mississippi and Atchafalaya sediment on the Texas–Louisiana shelf: Model estimates for the year 1993. Cont. Shelf Res. 31, 1558–1575. http://dx.doi.org/10.1016/j.csr.2011.05.008.

Xu, K., Milliman, J.D., Li, A., Paul Liu, J., Kao, S.-J., Wan, S., 2009. Yangtze- and Taiwan-derived sediments on the inner shelf of East China Sea. Cont. Shelf Res. 29, 2240–2256. http://dx.doi.org/10.1016/j.csr.2009.08.017.

Xu, K., Li, A., Liu, J.P., Milliman, J.D., Yang, Z., Liu, C.-S., Kao, S.-J., Wan, S., Xu, F., 2012. Provenance, structure, and formation of the mud wedge along inner continental shelf of the East China Sea: a synthesis of the Yangtze dispersal system. Mar. Geol. 291–294, 176–191. http://dx.doi.org/10.1016/j.margeo.2011.06.003.

Yanagi, T., Takahashi, S., Hoshika, A., Tanimoto, T., 1996. Seasonal variation in the transport of suspended matter in the East China Sea. J. Oceanogr. 52, 539–552. http://dx.doi.org/10.1007/BF02238320.

Yang, S.Y., Jung, H.S., Lim, D.I., Li, C.X., 2003. A review on the provenance discrimination of sediments in the Yellow Sea. Earth-Sci. Rev. 63, 93–120. http://dx.doi.org/10.1016/S0012-8252(03)00033-3.

Yang, Z., Guo, Z., Wang, Z., Xu, J., Gao, W., 1992. The transport pattern of suspended material from the continental self of Yellow and East China Seas to the deep ocean. Acta Oceanol. Sin. 14, 81–90.

Yuan, D., Zhu, J., Li, C., Hu, D., 2008. Cross-shelf circulation in the Yellow and East China Seas indicated by MODIS satellite observations. J. Mar. Syst. 70, 134–149. http://dx.doi.org/10.1016/j.jmarsys.2007.04.002.

Zeng, X., Guan, W., Pan, C., 2011. Cumulative influence of long term reclamation on hydrodynamics in the Xiangshangang Bay. J. Mar. Sci., 73–83.

Zhang, J., 1995. Geochemistry of trace metals from Chinese river/estuary systems: an overview. Estuar. Coast. Shelf Sci. 41, 631–658. http://dx.doi.org/10.1006/ecss.1995.0082.

Zhang, J., 1999. Heavy metal compositions of suspended sediments in the Changjiang (Yangtze River) estuary: significance of riverine transport to the ocean. Cont. Shelf Res. 19, 1521–1543. http://dx.doi.org/10.1016/S0278-4343(99)00029-1.